Supramolecular barrels from amphiphilic rigid–flexible macrocycles

WON-YOUNG YANG, JONG-HYUN AHN, YONG-SIK YOO, NAM-KEUN OH AND MYONGSOO LEE*

Center for Supramolecular Nano-Assembly and Department of Chemistry, Yonsei University, Seoul 120-749, Korea

*e-mail: mslee@yonsei.ac.kr

Published online: 17 April 2005; doi:10.1038/nmat1373

Precise control of supramolecular objects requires the rational design of molecular components, because the information determining their specific assembly should be encoded in their molecular architecture[1–4]. In this context, diverse self-assembling molecules including liquid crystals[5], dendrimers[6], block copolymers[7], hydrogen-bonded complexes[8] and rigid macrocycles[9] are being created as a means of manipulating supramolecular structure. Incorporation of a stiff rod-like building block into an amphiphilic molecular architecture leads to another class of self-assembling molecules[10]. Aggregation of rod building blocks can generate various nanoscale objects including bundles[11,12], ribbons[13], tubules[14,15] and vesicles[16], depending on the molecular structure and/or the presence of a selective solvent. We present here an unusual example of supramolecular barrels in the solid and in aqueous solution, based on the self-assembly of amphiphilic rigid–flexible macrocycles driven by non-covalent interactions. Preliminary experiments show that these amphiphilic macrocycles are membrane-active. The amphiphilic macrocycles might thus lead to an excellent model system for exploring biological processes in supramolecular materials.

The macrocyclic molecules that form these aggregates consist of a hexa-*p*-phenylene rod and a poly(ethylene oxide) chain that are fused together into a macrocyclic ring (Fig. 1). The precursors of the macrocycles were prepared from the etherification of the corresponding poly(ethylene oxide)-terminated hexa-*p*-phenylenes with allyl chloride according to standard procedures[17]. The precursors were converted to macrocycles by ring-close metathesis reactions[18] under refluxing dichloromethane solution (0.005 M concentration) to produce the corresponding cyclic molecules (*cis*/*trans* ratio = 2/1) with reasonable yields. The resulting rod–coil macrocyclic molecules were characterized by ^{1}H and ^{13}C-NMR spectroscopy, elemental analysis and mass spectroscopy (matrix-assisted laser desorption ionization time-of-flight: MALDI-TOF), and shown to be in full agreement with the structures presented. The polydispersity index of the macrocyclic molecules measured by gel-permeation chromatography with the use of polystyrene standards was less than 1.05 (see Supplementary Information, Fig. S2). As expected, the macrocyclic molecules were observed to elute at higher elution volume than the linear precursor[19]. Number-averaged relative molecular masses ($\bar{M}_n$)

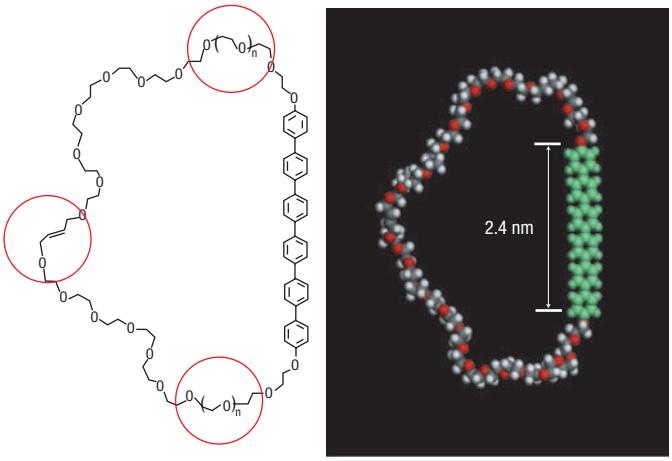

Figure 1 Chemical structure of a rigid–flexible macrocycle. Schematic molecular structure of an amphiphilic rigid–flexible macrocycle and thermal transitions (°C) (rec, rectangular; ortho, orthorhombic; tet, tetragonal; cub, cubic; i, isotropic; obl, oblique; f_{coil}, coil fraction). Upper right: CPK model of **1**.

of molecules **1** and **2**, which differ in the length of the flexible chain, were observed to be 1,950 and 2,460 by MALDI-TOF mass spectroscopy (Supplementary Information Fig. S3).

The transition temperatures of **1** and **2** determined from differential scanning calorimetry heating and cooling scans are summarized in Fig. 1. Both **1** and **2** were observed to undergo double phase transitions in the crystalline state and to form ordered mesophases at higher temperature as confirmed by differential scanning calorimetry (Supplementary Information Fig. S4). After

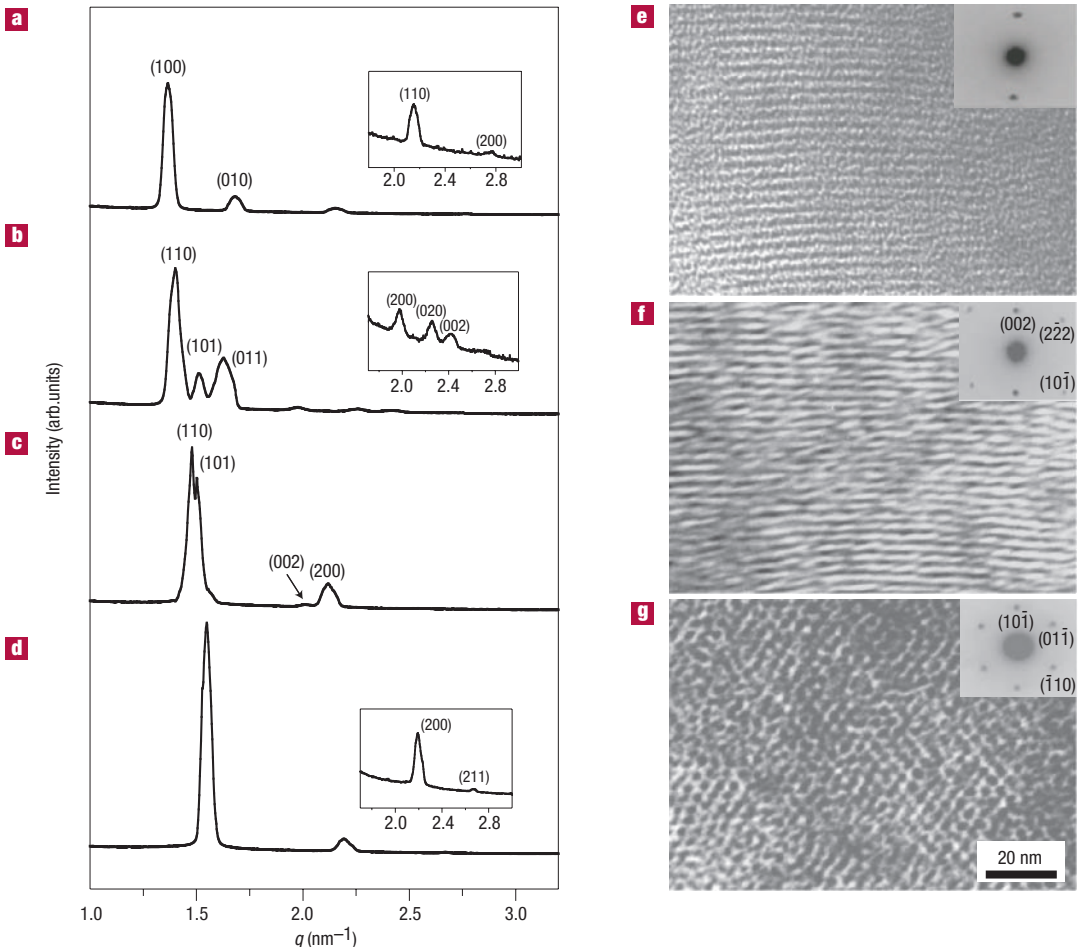

Figure 2 Structural data of rigid–flexible macrocycles. **a–d**, Small-angle X-ray diffraction patterns of **1**. **a**, Two-dimensional rectangular structure with lattice parameters $a = 4.6$ nm and $b = 3.7$ nm at 25 °C; **b**, three-dimensional body-centred orthorhombic structure with lattice parameters $a = 6.5$ nm, $b = 5.8$ nm, and $c = 5.3$ nm at 80 °C; **c**, three-dimensional body-centred tetragonal structure with lattice parameters $a = b = 6.1$ nm and $c = 5.9$ nm at 110 °C, and **d**, three-dimensional body-centred cubic structure with lattice parameter $a = 5.7$ nm at 150 °C. **e–g**, TEM images of **1**. $q = 4\pi\sin\theta/\lambda$. **e**, Two-dimensional rectangular structure, with electron diffraction pattern shown in the inset. **f**, Three-dimensional body-centred orthorhombic structure; the electron diffraction pattern in the inset shows {002} and {222} reflections from [110] projection. **g**, Three-dimensional body-centred tetragonal structure; the electron diffraction pattern in the inset shows {110} reflections from [111] projection.

the second crystal melting transition, **1** showed a birefringent mesophase, followed at higher temperature by an optically isotropic cubic mesophase, whereas **2** displayed only an optically isotropic cubic mesophase.

The small-angle X-ray scattering of **1** at ambient temperature showed several sharp reflections that corresponded to a two-dimensional (2D) rectangular structure (Fig. 2a), whereas **2** showed a similar diffraction pattern that could be indexed as an oblique lattice with a characteristic angle of 100°. The 2D structure of **1** (stained with RuO_4) was further confirmed by transmission electron microscopy (TEM) which shows organized, dark, more stained 1D aromatic domains with a thickness of 2.5 nm (Fig. 2e). Considering the cyclic molecular structure and aromatic rod length (2.4 nm by CPK modelling), the dark aromatic domains in the image suggest a laterally coupled bilayer ribbon structure in which the rod segments face each other (Fig. 3a). The cyclic geometry of the coil attached to one side of the rod would prohibit the 2D growth of a self-assembled structure. Instead, the aromatic rod segments should be strongly driven to aggregate in one dimension to produce a laterally stacked bilayer through microphase separation between the rod and coil segments, and π–π interactions[11,20]. The π–π stacking interactions are reflected in the wide-angle X-ray scattering peak at a q-value of about 14.6 nm^{-1} (Supplementary Information Fig. S6). Thus, these would lead to infinitely long ribbon-like 1D aggregates with uniform width and thickness.

On heating, **1** and **2** showed a large number of reflections including three strong reflections in the lower angles, suggesting the presence of a highly ordered nanoscopic structure with three distinct lattice parameters (Fig. 2b). These reflections can be indexed as a 3D body-centred orthorhombic structure with three distinct dimensions. The wide-angle X-ray scatterings revealed a reflection at a q-value of about 14.3 nm^{-1} (Fig. S6), which is due to crystal packing of the rod segments within the domains. When microtomed films of **1** stained with RuO_4 after annealing at 80 °C were characterized by TEM, an ordered array of discrete dark aggregates in the matrix of aliphatic chains could be observed (Fig. 2f). The image and small-angle electron diffraction pattern in Fig. 2f revealed that the shape of the aggregates is discrete oblate with axes of roughly 8 and 2 nm, which are comparable to the dimensions determined from the 3D lattice parameters and the densities.

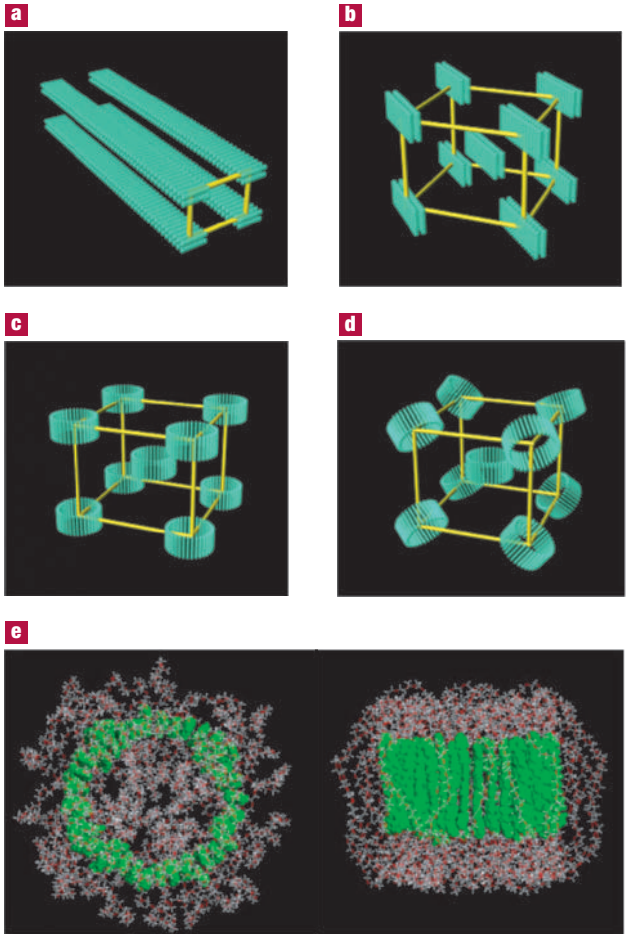

Figure 3 Supramolecular architectures from self-assembly of rigid–flexible macrocycles. Schematic representation of **a**, 2D rectangular structure and **b**, 3D body-centred orthorhombic structure (*Imm*2) from ribbon-like aggregates; **c**, 3D body-centred tetragonal structure (*I*4/*mmm*) and **d**, 3D body-centred cubic structure ($Im\bar{3}m$) from barrel-like aggregates. Coil segments are omitted for clarity. **e**, Top view (left) and side view (right) of a barrel-like structure by molecular modelling of **1** (rod segments are coloured green, oxygens and hydrocarbons are coloured red and grey, respectively). The inner and outer diameter are calculated to be 3.2 and 4.0 nm, respectively.

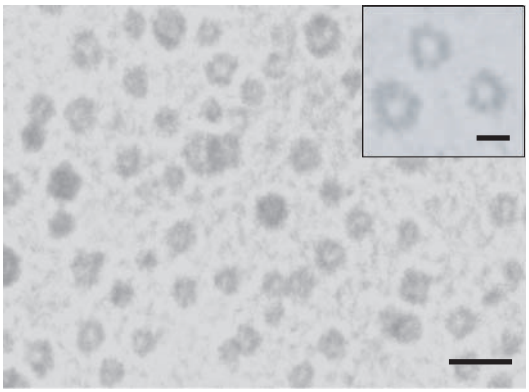

Figure 4 TEM image of barrel-like tubular structures in an aqueous solution. The sample was prepared by dropping the solution onto a carbon grid, air-drying and then staining with RuO_4 before observation. The scale bar represents 20 nm. Inset: higher-magnification image showing contrast between the periphery and centre. The dark areas arise because the rod segments are more stained than the coils. The scale bar represents 5 nm.

On the basis of the X-ray diffraction and TEM results, the rod segments can be considered to self-assemble into discrete ribbon-like aggregates with a laterally stacked bilayer encapsulated by cyclic aliphatic chains in which the rod building blocks are arranged with their long axes parallel to each other. Subsequently, the ribbon nanostructures self-organize into a 3D body-centred orthorhombic superlattice (Fig. 3b). Both steric forces and crystallization of the rod segments are believed to play an important part in the formation of discrete ribbons[21]. The tendency of the rod building blocks to pack into a parallel arrangement accompanies a strong coil deformation on heating. To reduce the energetic penalty associated with coil deformation, while maintaining crystalline order of the rod segments, infinitely long ribbons would break up into discrete ribbons that allow coils to splay at the periphery of the supramolecular unit. The anisotropic crystalline order of the rod segments seems to generate non-curved discrete aggregates, as shown by the wide-angle X-ray diffraction peak at q-value of about 14.3 nm^{-1}.

In the birefringent mesophase of **1**, small-angle X-ray scattering showed several reflections (Fig. 2c), corresponding to a 3D body-centred tetragonal superlattice with lattice parameters of 6.1 and 5.9 nm, whereas wide-angle scattering showed only a broad halo (Supplementary Information Fig. S6), indicative of liquid crystalline order of the rod segments within domains. On cooling from the optically isotropic mesophase, straight lines growing in four directions with an angle of 90° could be observed in the polarized optical microscope (Supplementary Information Fig. S7) with a final development of mosaic texture, indicative of the presence of a 3D non-cubic lattice[22]. On further heating to the optically isotropic mesophase, the small-angle X-ray scattering pattern (Fig. 2d) showed three sharp peaks that could be indexed as a 3D body-centred cubic phase with a lattice parameter of 5.7 nm. Similar to the optically isotropic mesophase of **1**, **2** in the mesophase showed several reflections corresponding to a 3D body-centred cubic structure with a lattice parameter of 6.7 nm.

To further confirm the mesophase structure, we investigated **1** in the birefringent mesophase by TEM. Micrographs of cryo-ultramicrotomed films (stained with RuO_4) after annealing at 120 °C showed a regular array of darker-stained rod domains in a matrix of light coil segments (Fig. 2g). These results together with the small-angle X-ray scattering demonstrate that the molecules in the molten state self-assemble into discrete nanostructures that organize into a 3D body-centred tetragonal superlattice (Fig. 3c). The image and electron diffraction pattern showed a regular array of dark spots with a rectangular lattice. Thus, the aggregates shown in the image are positioned at the lattice points on a (110) plane of the 3D body-centred tetragonal superlattice. To gain insight into the internal structure of the aromatic domains, we calculated the number of molecules per aggregate by using the lattice constants and densities. Aggregates of **1** were estimated to contain about 40 molecules each. Considering microphase separation between the rod and coil segments, the aggregation of 40 rod–coil macrocyclic molecules in an aggregate can be viewed as generating a barrel-like supramolecular structure in which the rods are aligned axially with their preferred direction, and both the interior and exterior of the barrel are filled by the coil segments (Fig. 3e). The formation of discrete barrels is also illustrated by a computer model in which the COMPASS empirical force-field calculation was used on a cluster of 40 molecules arranged parallel to each other. Figure 3e shows the cluster of cyclic molecules

after complete energy minimization, suggesting that a barrel-like structure is energetically favourable. The calculation showed that the external diameter is 4.0 nm, which is consistent with the size of the dark aggregates in the TEM image. In addition, the calculation showed that the internal diameter and the length are estimated to be 3.2 and 2.4 nm, respectively. On further heating of **1**, the non-cubic 3D order of the barrels transforms into a 3D body-centred cubic order (Fig. 3d).

These results indicate that a flat discrete ribbon-like aggregate transforms into a curved barrel-like structure on crystal melting of the rod segments. This transformation may be rationalized by considering end-to-end connection by rolling of the discrete ribbon[23]. With increasing temperature, space crowding of coil segments would be larger because of greater thermal motion of the flexible chains. A ribbon-like ordering of the rod segments would confine flexible coil segments to a flat interface, forcing a strong deformation of the flexible coils and making the system energetically unfavourable. To release this deformation without sacrificing anisotropic order of the rod segments, the flat ribbons would roll to form curved barrels.

Self-assembly of the rod–coil macrocycles into a barrel structure with hydrophilic exterior and interior in bulk suggests that they may also assemble into a similar structure in aqueous solution[24]. We therefore studied aggregation behaviour of the macrocycles in water by using dynamic light scattering. Our studies showed that **1** self-assembles into discrete aggregates of uniform size (Supplementary Information Fig. S8). The average diameter of the aggregates was observed to be about 7 nm, which is larger than that in bulk. Further evidence for the formation of the aggregates in **1** was provided by TEM experiments (Fig. 4). Notably, the images revealed that there is obvious contrast between the periphery and centre in the object, characteristic of the projection images of hollow cylinders. The diameter of the internal pore was measured to be about 2 nm. The hollow cylindrical image is believed to be the result of the formation of a barrel-like tubular structure with a water-filled pore.

Preliminary transport experiments indicate that the amphiphilic macrocycles are active in lipid bilayer membranes (see Supplementary Information). The results suggest that this class of self-assembling molecules may allow the design of a variety of well-defined organic nanostructures with biological functions.

METHODS

Reagents used were *p*-toluenesulphonyl chloride (98%) and triphenylphosphine (99%) (Tokyo Kasei, as received); poly(ethylene glycol) ($\bar{M}_n$ = 600 and 900), allyl chloride (98%), 4′-bromo-[1,1′-biphenyl]-4-ol (97%), 8-hydroxypyrene-1,3,6-trisulphonic acid (HPTS) (Aldrich); benzylidene-bis-(tricyclohexylphosphine)-dichlororuthenium (Fluka); egg yolk L-α-phosphatidylcholine and cholesterol (Avanti Polar Lipids). The other conventional reagents were used as received.

Dynamic light scattering measurements were made with an ALV/CGS-3 Compact Goniometer System. X-ray scattering measurements were made in transmission mode with synchrotron radiation at the 3C2 X-ray beam line at Pohang Accelerator Laboratory, Korea. To investigate structural changes on heating, the sample was held in an aluminium sample holder, which was sealed with two 7-mm-thick Kapton films that form a window. The sample was heated with two cartridge heaters and the temperature of the samples was monitored by a thermocouple placed close to the sample. A background scattering correction was made by subtracting the measured scattering from the Kapton.

Transmission electron microscopy was carried out at 120 kV using a JEOL-JEM 2010. Steady-state fluorescence spectra were obtained from a Hitachi F-4500 fluorescence spectrophotometer. Density (ρ) measurements of compounds were made in a mixture of *n*-hexane and CCl_4. Compounds were synthesized according to the procedure described in the Supplementary Information, scheme S1, and then purified by silica gel column chromatography and preparative high-pressure liquid chromatography (Japan Analytical Instruments).

Received 25 November 2004; accepted 18 February 2005; published 17 April 2005.

References

1. Lehn, J.-M. Supramolecular chemistry and self-assembly special feature. Toward complex matter: supramolecular chemistry and self-organization. *Proc. Natl Acad. Sci. USA* **99,** 4763–4768 (2002).
2. Whitesides, G. M. & Grzybowski, B. Self-assembly at all scales. *Science* **295,** 2418–2421 (2002).
3. Sarikaya, M., Tamerler, C., Jen, A. K.-Y., Schulten, K. & Baneyx, F. Molecular biomimetics: nanotechnology through biology. *Nature Mater.* **2,** 577–585 (2003).
4. Elemans, J. A. A. W., Rowan, A. E. & Nolte, R. J. M. Porosity of core–shell nanoparticles. *J. Mater. Chem.* **13,** 2661–2666 (2004).
5. Kato, T. Self-assembly of phase-segregated liquid crystal structures. *Science* **295,** 2414–2418 (2002).
6. Percec V. *et al.* Self-assembly of amphiphilic dendritic dipeptides into helical pores. *Nature* **430,** 764–768 (2004).
7. Föster, S. & Plantenberg, T. From self-organizing polymers to nanohybrid and biomaterials. *Angew. Chem. Int. Edn Engl.* **41,** 688–714 (2002).
8. Hirschberg, J. H. K. *et al.* Helical self-assembled polymers from cooperative stacking of hydrogen-bonded pairs. *Nature* **407,** 167–170 (2000).
9. Zhao, D. & Moore, J. S. Shape-persistent arylene ethynyene macrocycles: syntheses and supramolecular chemistry. *Chem. Commun.* **7,** 807–818 (2003).
10. Lee, M., Cho, B.-K. & Zin, W.-C. Supramolecular structures from rod–coil block copolymers. *Chem. Rev.* **101,** 3869–3892 (2001).
11. Stupp, S. I. *et al.* Supramolecular materials: self-organized nanostructures. *Science* **276,** 384–389 (1997).
12. Das, G. *et al.* β-Fibrillogenesis from rigid-rod β-barrels:hierarchical preorganization beyond microns. *Angew. Chem. Int. Edn* **40,** 4657–4661 (2001).
13. Zubarev, E. R., Pralle, M. U., Sone, E. D. & Stupp, S. I. Self-assembly of dendron rod–coil molecules into nanoribbons. *J. Am. Chem. Soc.* **123,** 4105–4106 (2001).
14. Park, S., Lim, J. -H., Chung, S.-W. & Mirkin, C. A. Self-assembly of mesoscopic metal-polymer amphiphiles. *Science* **303,** 348–351 (2004).
15. Hill, J. P. *et al.* Self-assembled hexa-peri-hexabenzocoronene graphitic nanotube. *Science* **304,** 1481–1483 (2004).
16. Vriezema, D. M. *et al.* Vesicles and polymerized vesicles from thiophene-containing rod–coil block copolymers. *Angew. Chem. Int. Edn Engl.* **42,** 772–776 (2003).
17. Lee, M., Jang, C. J. & Ryu, J.-H. Supramolecular reactor from self-assembly of rod-coil molecule in aqueous environment. *J. Am. Chem. Soc.* **126,** 8082–8083 (2004).
18. Fürstner, A. Olefin metathesis and beyond. *Angew. Chem. Int. Edn Engl.* **39,** 3012–3043 (2000).
19. Schappacher, M. & Deffieux, A. α-Acetal-ω-bis(hydroxymethyl) heterodifunctional polystyrene: synthesis, characterization, and investigation of intramolecular end-to-end ring closure. *Macromolecules* **34,** 5827–5832 (2001).
20. Wang, H., You, W., Jiang, P., Yu, L. & Wang, H. H. Supramolecular self-assembly of conjugated diblock copolymers. *Chem. Eur. J.* **10,** 986 (2004).
21. Williams, D. R. M. & Fredrickson, G. H. Cylindrical micelles in rigid–flexible diblock copolymers. *Macromolecules* **25,** 3561–3568 (1992).
22. Lee, M., Cho, B.-K., Jang, Y.-G. & Zin, W.-C. Spontaneous organization of supramolecular rod-bundles into a body-centered tetragonal assembly in coil–rod–coil molecules *J. Am. Chem. Soc.* **122,** 7449–7455 (2000).
23. In, M., Aguerre-Chariol, O. & Zana, R. Closed-looped micelles in surfactant tetramer solutions. *J. Phys. Chem. B* **103,** 7747–7750 (1999).
24. Bong, D. T., Clark, T. D., Granja, J. R. & Ghadiri, M. R. Self-assembling organic nanotubes. *Angew. Chem. Int. Edn Engl.* **40,** 988–1011 (2001).

Acknowledgements

We thank the National Creative Research Initiative Program of the Korean Ministry of Science and Technology for financial support of this work and the Pohang Accelerator Laboratory for synchrotron radiation experiments.

Correspondence and requests for materials should be addressed to M.L.

Supplementary Information accompanies the paper on www.nature.com/naturematerials.

Competing financial interests

The authors declare that they have no competing financial interests.